



Universiteit  
Leiden  
The Netherlands

## Photon detection at subwavelength scales

Wang, Q.

### Citation

Wang, Q. (2015, October 27). *Photon detection at subwavelength scales*. Retrieved from <https://hdl.handle.net/1887/35972>

Version: Not Applicable (or Unknown)

License: [Leiden University Non-exclusive license](#)

Downloaded from: <https://hdl.handle.net/1887/35972>

**Note:** To cite this publication please use the final published version (if applicable).

Cover Page



Universiteit Leiden



The handle <http://hdl.handle.net/1887/35972> holds various files of this Leiden University dissertation.

**Author:** Wang, Qiang

**Title:** Photon detection at subwavelength scales

**Issue Date:** 2015-10-27

## Chapter 2

# How Noise Affects Quantum Detector Tomography

We determine the full photon number response of a NbN superconducting nanowire single-photon detector via quantum detector tomography, and the results show the separation of linear, effective absorption efficiency from the internal detection efficiencies. In addition, we demonstrate an error budget for the complete quantum characterization of the detector. We find that for short times, the dominant noise source is shot noise, while laser power fluctuations limit the accuracy for longer timescales. The combined standard uncertainty of the internal detection efficiency derived from our measurements is about 2%<sup>1</sup>.

### 2.1 Introduction

The detection of single photons plays an important role in quantum optics [3] and quantum key distribution [50]. Superconducting single-photon detectors (SSPDs) for near-infrared wavelengths are promising because they combine high detection efficiency and high speed. In particular SSPDs made out of NbN and related materials have received a lot of attention because these detectors can be operated at relatively high temperatures of  $\sim 4$  K. Moreover, these detectors are technologically interesting due to a combination of high speed, low dark count rate, low jitter and high detection efficiency [17]. Typically, the detection efficiency and dark count rate are determined through

---

<sup>1</sup>Q. Wang, J. J. Renema, A. Gaggero, F. Mattioli, R. Leoni, M. P. van Exter, and M. J. A. de Dood, accepted by J. Appl. Phys. for publication.

measurement of the count rate as a function of the incident photon flux and detector bias current.

Further progress on characterizing SSPDs for applications in quantum optics can be made by using quantum detector tomography (QDT) [28, 34, 51–53] as a method to retrieve the complete quantum response of the detector. This assumption-free method is based on the calculation of the Positive Operator Valued Measure (POVM) [28, 34, 51–53], which mathematically determines the operator  $\{\Pi_{click}\}$  of the detector. The probability of a click event is expressed as:

$$R_{click} = \text{Tr}(\rho \Pi_{click}), \quad (2.1)$$

where  $\rho$  is the density matrix that describes the input state. Usually well-defined coherent states from a laser are used as probe states. Coherent states are a linear combination of photon number states (i.e., Fock states) with  $\rho = |N\rangle\langle N|$  and  $|N\rangle = \sum_{i=0}^{\infty} N^{\frac{i}{2}} \exp(-\frac{N}{2}) / \sqrt{i!} |i\rangle$  ( $N$  is the mean photon number of the coherent state and  $i$  indexes the photon number). In the basis of photon number states, the operator of the detector is written as  $\{\Pi_{click}\} = \sum_{i=0}^{\infty} \tilde{p}_i |i\rangle\langle i|$ , where  $\tilde{p}_i$  is the probability of a click event caused by an input photon number state  $|i\rangle$ . Because the detection is not phase-sensitive a description with only the diagonal elements of the POVM suffices. The description of SSPDs is further simplified by the fact that these detectors produce a binary response of “click” or “no-click” that does not contain information about the number of photons. We calculate first the no-click probability and then compute the click probability for a coherent state as [29, 36]:

$$\begin{aligned} R_{click}(N) &= 1 - R_{no-click}(N) \\ &= 1 - e^{-N} \sum_{i=0}^{\tilde{m}} (1 - \tilde{p}_i) \frac{(N)^i}{i!}. \end{aligned} \quad (2.2)$$

Equation (2.2) includes an assumption supported by experimental observations that at high input power the detector saturates with  $\tilde{p}_i = 1$  for  $i > \tilde{m}$ . For detectors with very low optical coupling efficiency  $\eta$ , Eq. (2.2) involves a large number of parameters  $\tilde{p}_i$ , i.e., of order  $\eta^{-1}$  for an ideal single-photon detector.

In our experiment we illuminate a meandering SSPD with an active area of  $5 \times 5 \mu\text{m}^2$  with a  $\sim 200 \mu\text{m}$  diameter optical beam, and we estimate an optical coupling efficiency  $10^{-3}$ . Consequently, we would have to determine  $10^3$  parameters  $\tilde{p}_i$ , making standard detector tomography an unrealistic task. This difficulty can be partly resolved by introducing a smoothing of adjacent  $\tilde{p}_i$ , through Tikhonov regularization [28] to effectively reduce the number of independent parameters. For very small values of optical coupling efficiency

the effect of this regularization becomes more prominent and complicates the interpretation of tomography. To alleviate these problems, we replace the mean photon number in the input beam  $N$  by the mean number of absorbed photons  $\eta N$ , and replace Eq. (2.2) by [29]

$$R(N) = 1 - e^{-\eta N} \sum_{i=0}^m (1 - p_i) \frac{(\eta N)^i}{i!}, \quad (2.3)$$

where  $\eta$  is interpreted as the effective absorption efficiency to describe the optical coupling process, and the parameters  $p_i$  now have the significance of representing the internal detection efficiency that an absorbed photon number state  $|i\rangle$  causes a click. The sum of Eq. (2.3) has much fewer terms and it is possible to obtain the values of  $p_i$  by performing a relatively simple experiment.

The introduction of Eq. (2.3) does not result in a loss of generality because all solutions to Eq. (2.2) are solutions to Eq. (2.3) for  $\eta = 1$ . Cases with  $\eta \neq 1$  result in an overdetermined system, where an additional assumption has to be invoked to identify the solution of physical significance. In this case, we use the sparsity in the  $p_i$  to select the solution which has the fewest  $p_i \neq 1$ . We note that  $\eta$  and  $p_1$  are separable in the experiment [35] due to the fact that  $\eta$  enters into the detection probability of higher-order photon numbers. This modified tomography procedure is particularly well suited for detectors where  $\eta \ll 1$  [29] and has been used to study the intrinsic quantum response of SSPDs to different photon number [29, 35–37] and to study the physics of the detection mechanism [30, 38].

In the experiment, the detector is illuminated with laser pulses that each contains a coherent state of light. The total detection probability is recorded as a function of average input power, which is proportional to the average photon number. Based on Eq. (2.3), an algorithm that takes into account the photon number distribution of the input states can be used to convert this information to an internal detection efficiency  $p_i$  in the photon number basis, which completely describes the detector.

The amount of information that can be extracted via tomography depends critically on the accuracy with which it is performed. For short measurement times the measured photon count rates show fluctuations that define a fundamental lower limit to the accuracy of the tomography. It is thus a natural question to ask how accurate QDT is in this limit and what other experimental factors limit the accuracy. A first estimate of the error in the nonlinear response of NbN superconducting detectors is reported in Ref. [30], and a calibration of the overall detection probability of an SSPD at high bias currents is reported in Ref. [54]. However, a discussion on the nature of the noise sources and how each of these sources affects the nonlinear detection probabilities determined by tomography has not been given.

In this chapter, we investigate the accuracy of quantum detector tomography on a meandering NbN SSPD. We consider five experimental factors: shot noise, fluctuations in laser power, non-linearities in the optical power meter, and fluctuations in bias current and temperature. We compare experimental results to synthesized data in order to systematically analyze how each noise factor influences QDT. By quantifying every type of noise in the measurement we calculate the combined uncertainty of the QDT results.

This chapter is structured as follows: Sections 2.2 and 2.3 describe the experiment and the method of quantum detector tomography, respectively. Section 2.4 contains the experimental results of QDT on an SSPD. In Section 2.5 we perform simulations to unravel the contribution of each noise source to QDT.

## 2.2 Experiment

The SSPD in this study is made out of a 4.5 nm thick NbN film deposited on a silicon substrate with a 254 nm thick layer of thermally grown SiO<sub>2</sub>. The NbN film is fabricated into a 100 nm wide, meandering wire, with 150 nm spacing between the wires (fill factor is 40%). The total active area of the device is  $5 \times 5 \mu\text{m}^2$ . The SiO<sub>2</sub> layer serves as a  $\lambda/4$  cavity optimized for 1550 nm wavelength. The critical current  $I_c$  of this device is measured to be  $23.5 \pm 0.5 \mu\text{A}$  at a temperature of 3.2 K corresponding to a critical current density  $j_c \approx 5.2 \times 10^6 \text{A}/\text{cm}^2$ .

The detector is mounted in a pulse-tube cryostat with free-space optical access (PRO-K-0274-00, Entropy GmbH), and is cooled down to a base temperature of 3.2 K. A bias current  $I_b$ , which is a significant fraction of the critical current  $I_c$  of the detector, is applied using a voltage source (Yokogawa GS200) with a 100  $\Omega$  resistor in series with the detector to convert the applied voltage to a bias current. Voltage pulses, which correspond to detection events, are collected via the high-frequency port of a bias-T (Minicircuits ZNBT-60-1W+) and are amplified via a cascade of high-frequency amplifiers ( $3 \times$  Minicircuits ZX60-3-18G+, 60 dB total amplification). The resulting pulses are sent to a pulse counter (Agilent 53131A).

To measure the detector response, the detector is illuminated in free space with picosecond laser pulses at a wavelength of  $\lambda = 1200 \text{ nm}$  from a spectrally filtered supercontinuum laser with a repetition rate of 20 MHz (Fianium FP 1060). For free-space illumination, the optical coupling efficiency (i.e., effective absorption efficiency  $\eta$ ) is mainly determined by the alignment and the ratio of the area of the meandering wire to the light spot size (diameter of  $\sim 200 \mu\text{m}$ ). The large beam diameter eliminates mechanical vibrations and drift of the optical alignment, but compromises the optical coupling efficiency

$\eta$ . We find that these effects are more important than the dependence of  $\eta$  on wavelength due to the enhanced absorption by the cavity resonance. We select the wavelength of 1200 nm rather than the preferred 1550 nm to achieve larger  $\eta$  and focus on the internal detection efficiency  $p_i$  for physical interpretation.

To filter the incident light we use a combination of a long pass filter, that transmits wavelengths beyond 1000 nm, and a band pass filter for 1200 nm wavelength light with a full-width-at-half-maximum of 10 nm. The mean photon number per pulse can be varied by rotating a half-wave plate placed in between two crossed polarizers. In this way, we tune the laser power (25 points) by a factor of  $\sim 600$  between the maximum and minimum while keeping the polarization of the incident light on the detector unaltered [42]. The observed count rate is recorded as a function of the mean photon number per pulse and bias current from 6.5  $\mu\text{A}$  to 16.8  $\mu\text{A}$ . At low bias current compared to the critical current, one can obtain the nonlinear response of the detector with relative ease. In these experiments we observe no dark count events in one second (i.e., dark count rate  $< 1$  Hz) up to the highest applied bias current of 16.8  $\mu\text{A}$ ; therefore, we neglect dark count rate for all bias currents. In order to investigate the influence of noise on QDT and to discriminate between shot noise and technical noise, we measure the count rate in 1000 consecutive intervals of 0.1 second at each setting of the optical power and bias current. This allows us to vary the integration time per point by averaging the data after the measurement.

## 2.3 Quantum detector tomography

The purpose of tomography is to find the detection probability expressed in the photon number basis. We apply the detector tomography protocol that was originally demonstrated in Ref. [28] with the modifications proposed in Ref. [29] for low system detection efficiency (see Eq. (2.3)). In the experiment, the number of detection events is recorded as a function of the mean number of photons per pulse, which is directly given by the average intensity of the laser and can be measured to a high degree of accuracy with a conventional power meter. Next, the tomography algorithm is applied, which processes the measured count rates to find a precise detector response as detection efficiencies expressed in the photon number basis.

In addition, in order to verify the separation of the effective absorption efficiency  $\eta$  and the internal detection efficiency  $p_i$ , we use two different settings of the input laser power, referred to as high power and low power. The low power was obtained by attenuating the high power using a neutral density filter that lowers the average power on the detector by a factor 2.51. The idea is that, according to the interpretation of Eq. (2.3), if the QDT for the data

(measured  $R$ ) with low laser power is performed by using the reference laser power before the attenuator (i.e., values of high power), the attenuation factor in the beam path will be attributed to the effective absorption efficiency  $\eta$  and will not affect the internal detection efficiency  $p_i$ .

Figure 2.1(a) shows a set of representative data used in tomography for both high and low laser power. Count rates are shown as a function of mean photon number per pulse for the two different input settings (solid curves for high power and dashed curves for low power); they are represented as a detection probability  $R$  by normalizing the count rate to the laser repetition rate (20 MHz). The mean photon number per pulse for the two settings of the laser power is calculated as  $N = P_L/(\hbar\omega f)$ , where  $P_L$  is the high or the low laser power,  $\omega$  is the angular frequency of the light at wavelength of 1200 nm, and  $f$  is the laser repetition rate. The total data set comprises measurements at 57 different bias currents. For clarity, we only plot the data for 4 bias currents in Fig. 2.1(a).

The data in Fig. 2.1(a) shows that the detector response is determined by both the bias current and the mean photon number  $N$ . The straight line with slope of 1 in the log-log plot for high bias currents (14.40  $\mu\text{A}$  and 16.05  $\mu\text{A}$ ) indicates that the detector behaves as a linear detector that saturates at large values of the mean photon number. When biased with a lower current, the detector shows a lower detection probability that increases more than linearly with mean photon number. A direct way to make this visible is by calculating the slope of the detection probability on a log-log scale as shown in Fig. 2.1(b).

At the highest bias current (16.05  $\mu\text{A}$ ) this slope is less than or equal to 1 and tends to 0 due to saturation of the detector at large  $N$ . For a lower bias current (14.40  $\mu\text{A}$ ), the detector response increases more than linearly for  $N > 10^2$  and then saturates. The higher-order nonlinear response is more prominent at the lower bias currents (8.48  $\mu\text{A}$  and 11.26  $\mu\text{A}$ ), where the derivative exceeds 2. Investigating these derivatives is a coarse method to identify the photon number response, from which it is not possible to quantify the probability to detect 1, 2 or 3 photons.

To quantify these probabilities, we implement the tomography as discussed in the Introduction to yield the values of effective absorption efficiency  $\eta$  and internal detection efficiency  $p_i$  of the measured detector. We fit Eq. (2.3) to the power dependent data at each current, and repeat the non-linear least-squares fitting procedure for different values of maximum photon number  $m$ . To determine the quality of the fit we calculate the reduced chi-squared  $\chi^2 = \chi_{\text{rough}}^2/v$ , where  $v$  is the number of degrees of freedom.

An essential feature of our tomography is that we select the model that minimizes the original, non-reduced  $\chi_{\text{rough}}^2$  and number of fit parameters, according to the Akaike Information Criterion  $AIC = \chi_{\text{rough}}^2 + 2s$  ( $s$  is the number

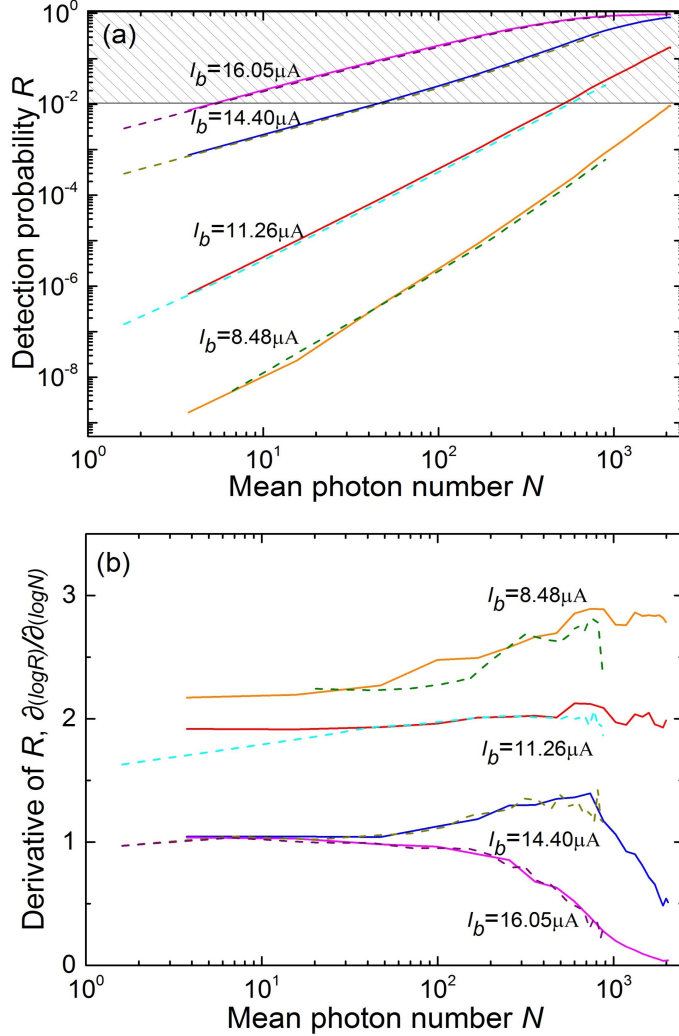


Figure 2.1: (a) Measured detection probability of the detector as a function of input photon number per pulse normalized to the laser repetition rate of 20 MHz. Data are shown for a high power setting (solid curves) and lower power (dashed curves) (b) Slope of the normalized count rate  $R$  on a log-log scale as a function of mean photon number  $N$  per pulse, giving a rough indication of the photon-number regime. At high bias currents ( $14.40 \mu\text{A}$  and  $16.05 \mu\text{A}$ ) the detector response is close to linear. For low bias currents ( $8.48 \mu\text{A}$  and  $11.26 \mu\text{A}$ ), the detector operates in a nonlinear regime.

of fitting parameters) [30, 55]. This criterion minimizes the number of parameters needed to describe a detector and is particularly useful for detectors with low efficiency [29]. We find that for the SSPD studied here, the dark count rate associated with  $p_0 (\sim 0)$  can be ignored and a description with only three parameters:  $\eta$ ,  $p_1$  and  $p_2$  suffices for all the bias currents.

It is important to stress again that the tomography put forward through Eq. (2.3) is completely general as it defines an (over)complete set of functions to describe the response of the detector. Alternative, more complex models can be defined that contain more detailed assumptions about the operation of the detectors. Such assumptions will alter the interpretation of the parameters in the model, but will not lead to a lower value of  $\chi^2$ . Therefore, we limit the discussion to the parameters that follow from the simplest possible complete model as defined through Eq. (2.3).

## 2.4 Overall noise and tomography results

In this section we analyze the noise in the measured data before starting a discussion on the influence of noise on the results of QDT. A straightforward way to show the noise is to quantify the statistical fluctuations of the data. We calculate the standard error of the mean (*SEM*) of the measured detection probability  $R$  for different integration times as a function of  $R$ , and normalize the *SEM* to the expected shot noise limit of the experimental data with an integration of 0.5 second. We normalize the *SEM* to this value, because a 0.5 second integration time together with the repetition rate  $f = 2 \times 10^7$ /s of our laser is comparable to the setting used in other tomography experiments on SSPDs [30, 37]. The shot noise limit is given by  $\sqrt{R(1-R)/tf}$ , with the integration time  $t$ , as predicted by the binomial distribution for a sequence of  $tf$  independent experiments.

We take the experimental data of high laser power setting as an example. Figure 2.2 shows the *SEM* of the data at all values of bias current for different integration times. The four drawn curves serve to guide the eye and are obtained by averaging every 100 points in each data set. As the integration time increases the overall *SEM* of the data decreases, as expected with a factor of  $1/\sqrt{n}$ , where  $n$  is the ratio of the integration time to the reference of 0.5 second.

For larger integration times, typically beyond  $\sim 1$  second per point, it becomes most clearly apparent that the total noise in the measurements exceeds the shot noise level (horizontal lines) by a factor 4–5 when the detection probability  $R$  is above  $10^{-2}$ . This means that at longer integration times the experimental tomography is limited by both shot noise and technical noise. At very high count rates, close to saturation, the detector response may be

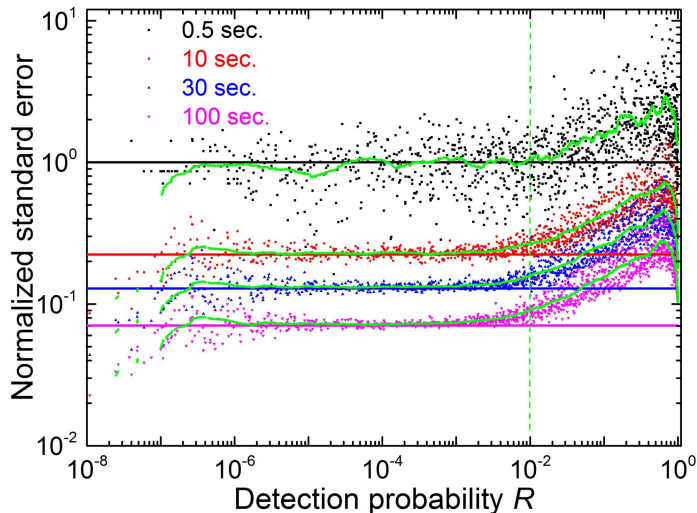


Figure 2.2: The ratio of the standard error of the mean of the data (high laser power setting) to the shot noise of the data with integration time of 0.5 second at all values of the bias current for different integration times.

influenced by heating effects [33, 56], which are not included in the detector response given by Eq. (2.3). Experimentally, we observe that the outcome of the tomography depends on the maximum photon count rate that is included in the fit procedure.

In order to exclude physical effects that go beyond the description from Eq. (2.3) we limit the data analysis to detection probabilities  $R$  below the value of  $10^{-2}$  (the left region of the vertical line in Fig. 2.2). This also excludes a large portion of the technical noise from the analysis. For practical tomography it is important to identify this threshold and find a tradeoff ( $10^{-2}$  in our case) between the error introduced by a too high threshold value and statistical errors introduced by a too low threshold value.

Figure 2.3 shows the quality of our fit  $\chi^2$  (based on the data of high laser power setting) on the left vertical axis as a function of the bias current for different maximum number of photons  $m$  in Eq. (2.3) up to 4. The figure indicates that a model with  $m = 2$  yields a good description of the data with a minimal set of fitting parameters ( $\eta$ ,  $p_1$  and  $p_2$ ), indicating that for  $i \geq 3$ , the internal efficiency  $p_i$  equals to 1, as desired.

In Fig. 2.3 the reduced  $\chi^2$  can be obtained only below the bias current of  $\sim 14 \mu\text{A}$ , this is due to the fact that the data of  $R$  above  $10^{-2}$ , corresponding to the shadowed data at bias currents  $> 14 \mu\text{A}$  in Fig. 2.1, are cut off and do not contribute to the QDT.

In the calculation of the reduced  $\chi^2$  we use the standard deviation  $\sigma_R$  of

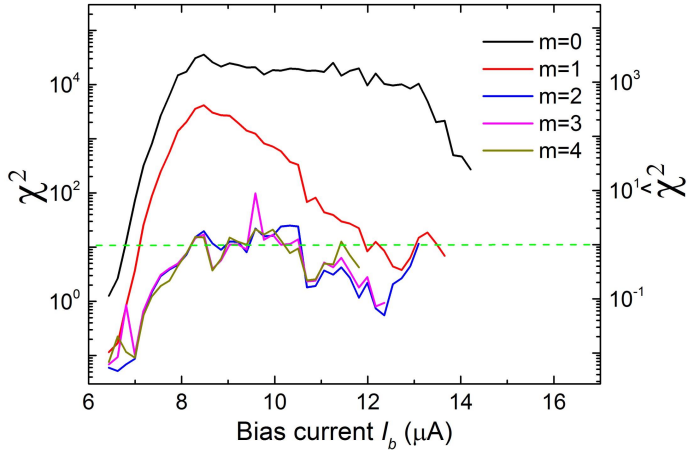


Figure 2.3: The reduced  $\chi^2$  and normalized  $\hat{\chi}^2$  from fitting the data to Eq. (2.3) at values of the detection probability  $R$  below  $10^{-2}$ . The reduced  $\chi^2$  is calculated based on the standard deviation of the raw data of  $R$ , while the normalized  $\hat{\chi}^2$  is based on the corrected standard deviation of  $R$  by including the long timescale fluctuations of the laser power.

the selected measured detection probability  $R$ . We find that the value of  $\chi^2$  is around  $\sim 10$  for currents from  $8 \mu\text{A}$  to  $11 \mu\text{A}$  while a good fit is supposed to have a  $\chi^2$  of 1.

The larger value of  $\chi^2$  can be interpreted as an underestimation of the standard deviation  $\sigma_R$  of the measured data. The standard deviation  $\sigma_R$  only shows the fluctuations in the data over a relatively short timescale of 100 seconds for each data point and ignores fluctuations or drifts in laser power on a longer timescale. In the next section we will show that a realistic estimate of this long term drift enlarges the  $\sigma_R$  by a factor of 3.3. Normalizing  $\chi^2$  by this value of  $\sigma_R$  leads to a  $\hat{\chi}^2 \sim 1$ , as shown in the right vertical axis in Fig. 2.3.

We emphasize that the QDT for both laser power settings was done using the reference power before the attenuator in order to verify that  $p_i$  and  $\eta$  can be determined as independent variables and that the value of  $\eta$  is lowered by the attenuation factor in the experiment. Figure 2.4(a) shows the internal detection efficiency  $p_1$  and  $p_2$  for a wavelength of 1200 nm as a function of bias current via tomography. We find that  $p_1$  and  $p_2$  for the two different powers are identical and are not influenced by the laser power setting, which confirms the separation between the internal detection process ( $p_i$ ) and the optical coupling process ( $\eta$ ). Meanwhile, the data of  $p_i$  shows the photon number regime that the detector operates in, e.g., below bias current of  $11 \mu\text{A}$  corresponding to 1-photon detection regime and above  $12 \mu\text{A}$  to 2-photon detection regime.

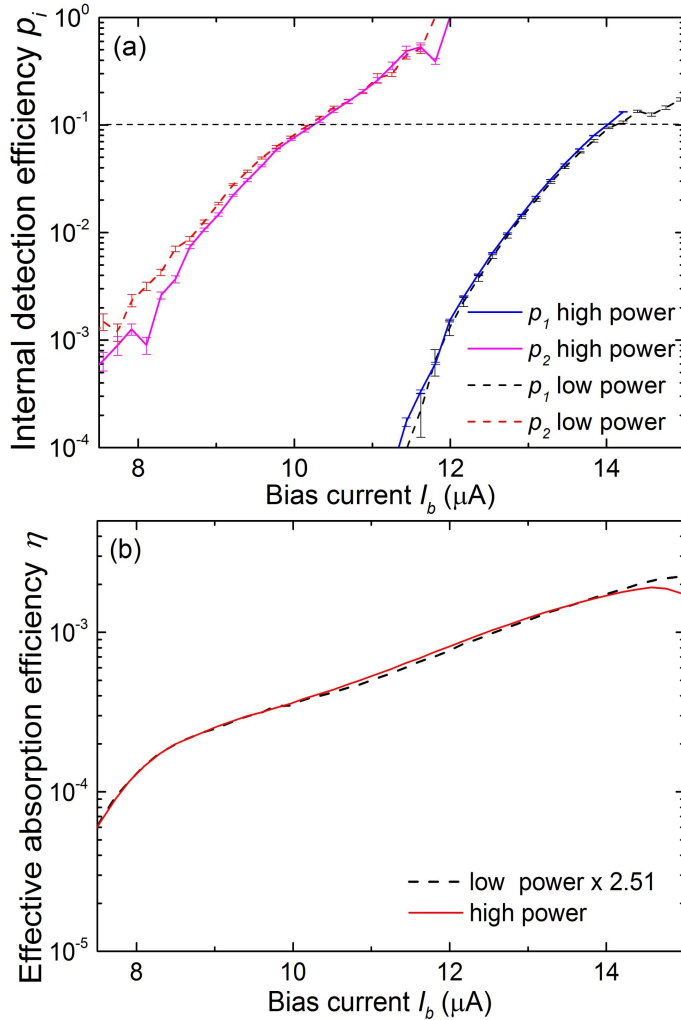


Figure 2.4: (a) Probabilities  $p_1$  and  $p_2$  of the NbN detector as a function of bias current determined by detector tomography. The horizontal line is used to calculate the relation between bias current and input photon energy in Section 2.5.6. (b) Effective absorption efficiency  $\eta$  for a photon participating in a detection event. Two sets of results are shown, corresponding to measurements at the two different input powers. The  $\eta$  for the low power is multiplied by 2.51, which is the attenuation factor in the beam path for the low power or the ratio of the high power to the low power input. The overlap between the curves ( $p_i$  and  $\eta$ ) demonstrates that the tomographic procedure retrieves the internal detection efficiencies that are intrinsic to the nature of the SSPD and separates them from the effective absorption efficiency.

The data in Fig. 2.4(b) shows the effective absorption efficiency  $\eta$  as a function of bias current, where the curve of  $\eta$  of the lower power setting is multiplied by the attenuation factor 2.51 for comparison. As we expected, linear loss or attenuation in the optical coupling is equivalent to rescaling the value of  $\eta$ , which confirms one of the main assumptions made in Ref. [29] to adapt detector tomography to detection systems with low efficiency.

In a straightforward interpretation of the detector tomography model a change in the value of  $\eta$  should not affect the retrieved values of  $p_1$  and  $p_2$ , because the values of  $p_i$  are interpreted as internal efficiencies that are related to the intrinsic detection mechanism of the NbN detector, while  $\eta$  is related to the coupling efficiency of a photon in the whole measurement system.

For an extended detector such as a meandering wire, the linear efficiency in the multiphoton regime is decreased because of the effect that two or more photons need to be absorbed close together to form a detection event [36, 57, 58]. Moreover  $\eta$  contains the optical absorption, inhomogeneities in the detector, the effect of bends and other factors that complicates further interpretation of this parameter. We restrict ourselves to the more straightforward interpretation to these intrinsic probabilities  $p_i$ .

## 2.5 Uncertainty budget and accuracy of tomography

### 2.5.1 Method of analyzing the uncertainty

Both shot noise and technical imperfections lead to fluctuations in the measured count rate that affect the value of  $p_i$  retrieved from tomography. We focus on the intrinsic detection probabilities  $p_i$ , quantify the fluctuations in the experiment, and discuss their origin and their consequences for the uncertainty of the  $p_i$  obtained from tomography. To simplify this task we will assume that all fluctuations are independent so that the uncertainty of  $p_i$  can be estimated by adding the uncertainty from each source.

We consider the effect of shot noise, fluctuations in laser power, nonlinearities in the optical power meter, instabilities of bias current and temperature. We use the tomography results at a bias current of 10.33  $\mu\text{A}$  and 14.00  $\mu\text{A}$  as an example, corresponding to a current setting where the detector operates in the two-photon regime and the one-photon regime, respectively.

We calculate the influence of the noise on the QDT results ( $p_i$ ) in two ways. For fluctuations of current and temperature we perform analytical error propagation based on the measured relation between  $p_i$  and  $I_b$ . For shot noise, laser power fluctuations and power meter instability, the relation between noise and  $p_i$  is more difficult to analyze due to the nonlinearity of Eq. (2.3). Therefore we

Table 2.1: The noise sources and the combined relative uncertainty.

Uncertainty source	Symbol	@ 10.33 $\mu\text{A}$ $p_1 = 0^*$ , $p_2 = 0.1$ ( $\eta = 4.09 \times 10^{-4}$ )	@ 14.00 $\mu\text{A}$ $p_1 = 0.1$ , $p_2 = 1^*$ ( $\eta = 1.71 \times 10^{-3}$ )
Shot noise ( $\propto 1/\sqrt{n}$ )	$u_S$	$3 \times 10^{-4}$	$0.4 \times 10^{-4}$
Laser power ( $\sigma_L = 2.8\%$ )	$u_L$	$9 \times 10^{-4}$	$16 \times 10^{-4}$
Power meter ( $\sigma_M = 0.9\%$ )	$u_M$	$0.5 \times 10^{-4}$	$0.3 \times 10^{-4}$
Bias current ( $\Delta I = 5.0 \text{ nA}$ )	$u_I$	$6 \times 10^{-4}$	$8 \times 10^{-4}$
Temperature ( $\Delta T = 4 \text{ mK}$ )	$u_T$	$6 \times 10^{-4}$	$9 \times 10^{-4}$
Combined uncertainty	$u = \sqrt{\sum_{k=1} u_k^2}$	$13 \times 10^{-4}$	$20 \times 10^{-4}$
Relative combined uncertainty	$U = u/p_i$	1.3%	2.0%

\*At current of 10.33  $\mu\text{A}$ , the detector is in 2-photon regime, where  $p_2 = 0.1$  and  $p_1$  is too low to be extracted from QDT; at current of 14.00  $\mu\text{A}$ , the detector is in 1-photon regime with  $p_1 = 0.1$ , and  $p_2$  fixed to 1.

perform numerical simulations<sup>2</sup>: we produce synthetic data of  $R_s$  with initial values of the tomography results (noted as  $\Pi_i$ ) at the two example currents. In this process we add noise to the synthetic data; then we perform tomography on these synthetic data and obtain the output (noted as  $P_i$ ); finally we obtain the uncertainty of the tomography results by calculating the difference between the initial ( $\Pi_i$ ) and the output values ( $P_i$ ). With these simulations we are able to evaluate how each of the noise sources (shot noise, laser power fluctuations and power meter instability) affects the tomography. The uncertainty of  $p_i$  caused by each noise source is summarized in Table 2.1. Details of the calculations are in section 2.5.2–2.5.7.

### 2.5.2 Shot noise

The fluctuations (or standard error of the mean) of a measured probability are fundamentally limited by statistical fluctuations of the discrete photon counting events. The standard error of the mean is predicted by binomial theory. To estimate how shot noise influences the final QDT results in our case, we perform tomography on synthetic data. As an example we use the experimental data at a bias current of 10.33  $\mu\text{A}$ , where  $p_1 = 0$ ,  $p_2 = 0.1$  and

<sup>2</sup>Matlab 2014b 64bits, The MathWorks, Inc.

$\eta = 4.09 \times 10^{-4}$ . In the simulation we take these initial values of  $p_i$  to be exact and denote these probabilities as  $\Pi_1$  and  $\Pi_2$ .

We first calculate the synthetic detection probability  $R_s$  as a function of the measured laser power by using Eq. (2.3), setting the  $\Pi_i$  and  $\eta$  values. We then add a noise term of  $r \times \sqrt{R_s(1-R_s)/tf}$  to  $R_s$  with  $tf = 2 \times 10^6$ ;  $r$  is a random number drawn from a Gaussian distribution with mean 0 and standard deviation 1. Then we repeat  $L = 1000$  times to produce  $L$  sets of detection probability.

On each set of synthetic data we perform tomography to retrieve values  $P_i$  for the internal detection efficiency  $p_i$ . We find that the value of  $P_1$  is indeed equal to 0, and we estimate the set of nonlinear parameters  $P_2$ , which may be different from the initial value  $\Pi_2$  that we set in the simulation. From these tomography simulations we extract the standard deviation  $\sigma_{pS}$  of the simulated  $P_2$ :

$$\sigma_{pS} = \sqrt{\frac{1}{L} \sum_{j=1}^L (P_{2,j} - \overline{P_2})^2}, \quad (2.4)$$

and we find that  $\sigma_{pS} = 7.9 \times 10^{-3}$ . The calculated mean value  $\overline{P_2}$  defined as  $\frac{1}{L} \sum_{j=1}^L P_{2,j}$ , is found to be equal to  $\Pi_2$ , indicating that the shot noise does not cause a bias, as expected. The shot noise affects the measurements in all  $L$  sets of measurements, and we need to consider the amount ( $L$  sets) of the synthetic data in uncertainty calculation: the uncertainty of  $P_2$  given by shot noise is calculated as  $u_S = \sigma_{pS} / \sqrt{L} = 3 \times 10^{-4}$ .

### 2.5.3 Laser power fluctuations

To estimate the magnitude and timescale of laser power fluctuations, we measure the laser power for 10 hours with a commercial Ge-based power meter (PH20-Ge, Gentec-EO).

Both short timescale fluctuations and long timescale drift in measured laser power are observed as shown in Fig. 2.5(a). The relative standard deviation of the measured laser power over the measurement of 10 hr is calculated to be  $\sigma_L = 2.8\%$  of the mean power. Figure 2.5(b) shows the autocorrelation function of the measured laser power of Fig. 2.5(a), and it demonstrates a long-timescale (of hours) fluctuation or drift of the laser power.

In the experiment of QDT, we vary laser power input using two polarizers, and fix a certain power (i.e., a fixed angle between two polarizers) into the cryostat and measure count rates as a function of detector bias current. We then repeat the measurement as a function of current for all input powers and convert the measured data to count rates as a function of input power at a fixed current. This data is then fed to the tomography algorithm. A consequence of

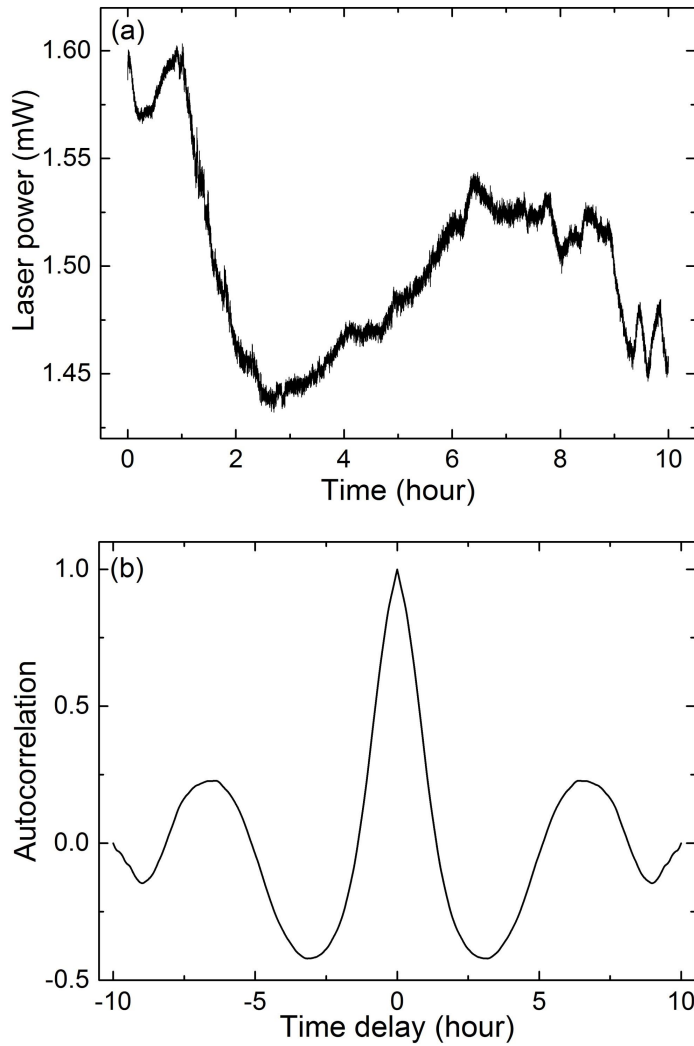


Figure 2.5: (a) Fluctuations in laser power output at 1200 nm wavelength as a function of time showing both fast fluctuations and long term drift with an amplitude of  $\sim 0.2$  mW over the whole timescale of 10 hours. (b) Corresponding autocorrelation function of laser power fluctuations.

this approach is that two adjacent points in the dataset are recorded approximately 1.6 hr after each other. At this timescale the autocorrelation function of the laser power fluctuations is close to zero, which means that laser power values are uncorrelated, and their fluctuations can be approximated as random. Each measured curve of count rate as a function of input power at constant current contains 25 points. During the measurement of each data point (100 seconds), the laser power is relatively constant because of the small standard deviation of 0.15% over this short time interval. Between the adjacent points with time interval of 1.6 hr, the long-timescale fluctuations of laser power are important (2.8%).

We assume that the power fluctuations are uncorrelated because the time interval between measurements is comparable to the timescale of the slow variations in laser power. To investigate to what extent the random laser fluctuations influence the tomography, we perform numerical simulations to take into account the nonlinear dependence of detection probability as a function of laser power as expressed by Eq. (2.3).

We use the data at the bias current of 10.33  $\mu\text{A}$  as an example. We first simplify the calculation by assuming that the fluctuations in the 25 laser power values are random. We add the random fluctuations to the calculation by multiplying each value with a factor of  $(1 + \sigma_L \times r)$ .

We then calculate one set of synthetic detection probability  $R_s$  by using Eq. (2.3), which involves the fluctuated laser power and the  $\Pi_i$  and  $\eta$  value. Finally, we do tomography to get the estimated  $\Pi_i$ . After repeating the procedure  $L$  times we have a set of simulated  $P_2$  with the mean value  $\bar{P}_2$  ( $P_1$  is equal to 0), and we calculate the bias of  $P_2$  as  $\Delta P_{2L} = \bar{P}_2 - \Pi_2 = 9 \times 10^{-4}$ , so we get the uncertainty of  $P_2$  given by laser power fluctuations  $u_L = \Delta P_{2L} = 9.4 \times 10^{-4}$ .

The long-timescale fluctuations ( $\sigma_L = 2.8\%$ ) of laser power are not included in the standard deviation  $\sigma_R$  of the measured data, so it leads to an underestimation of the noise of the data and increases the reduced  $\chi^2$ . We calculate the change in the measured detection probability  $R$  caused by fluctuations of the laser power (the mean photon number  $N$ ) as  $\Delta R = \frac{\partial R}{\partial N} \Delta N = \frac{\partial R}{\partial N} N \frac{\Delta N}{N}$  via Eq. (2.3), where we use the values of  $p_i$  and  $\eta$  at 10.33  $\mu\text{A}$ , and  $\frac{\Delta N}{N}$  is 2.8%. The results show that  $\Delta R$  is  $R$  dependent and is in a range of  $1 \times 10^{-4} - 4 \times 10^{-4}$ . We estimate the new overall fluctuations of the data in a simple way as  $\sigma'_R = \sqrt{\sigma_R^2 + \Delta R^2} = 3.3\sigma_R$  by using the averaged value  $\overline{\Delta R} = 2.5 \times 10^{-4}$ . With this correction for the overall fluctuations the QDT gives a lower  $\hat{\chi}^2$  of  $\sim 3$  at 10.33  $\mu\text{A}$ , which is suppressed from the value ( $\sim 40$ ) in the original QDT (see  $\chi^2$  in Fig. 2.3). We conclude that the long-timescale drift (e.g., in laser power) causes the larger values of  $\chi^2$ .

### 2.5.4 Accuracy of the power meter

The function of the power meter is to provide reference values of laser power that are inserted in the tomography. The power meter has an absolute accuracy that shifts all points equally and leads to a systematic error, which can be simply attributed to a change of  $\eta$ . In addition, the relative uncertainty of the power meter is limited by noise (e.g., dark count) of the power meter itself.

We record the laser power with a commercial Ge-based power meter (PH20-Ge, Gentec-EO) that has a specified relative uncertainty of  $\pm 0.3\%$  to  $\pm 0.9\%$  given by NIST [59]. In our simulation we take the upper limit (0.9%) as a conservative estimate of fluctuations in the readout of the power meter. To study the fast-fluctuation influence on the final  $p_i$ , we generate one set of detection probabilities with the original measured laser power values as the true values. Then in the fitting part we use a different calibration curve that contains the fluctuations in power measurement by multiplying each point of the original laser power with a factor of  $(1 + \sigma_M \times r)$ , where the  $\sigma_M$  equals 0.9%. We repeat this procedure  $L$  times and get a set of  $P_2$ . The difference of  $\Pi_2$  and  $\bar{P}_2$  is  $\Delta P_{2M} = 0.5 \times 10^{-4}$ , and the uncertainty of  $P_2$  given by power meter is  $u_M = \Delta P_{2M} = 0.5 \times 10^{-4}$ .

### 2.5.5 Current fluctuations

As can be seen in Fig. 2.4(a) the detection probabilities are strongly dependent on bias current. Based on the outcome of the tomography we find an empirical relation to describe the relevant part of the  $p_i$  curve. This empirical relation allows standard error propagation by calculating the sensitivity of the  $p_i$  to bias current fluctuations as the local derivative of the empirical curve. As an example we take  $p_2$  at a bias current of  $10.33 \mu\text{A}$  and fit the current dependence to the function:

$$p_2(I_b) = p_2(10.33\mu\text{A})e^{\alpha(I_b - 10.33\mu\text{A})}. \quad (2.5)$$

We obtain a value of  $p_2(10.33 \mu\text{A}) = 0.10$ , and the slope  $\alpha = 1.121 \pm 0.004 \mu\text{A}^{-1}$ . The influence of current fluctuations on the accuracy of  $p_2$  can be estimated from a Taylor expansion of Eq. (2.5) and yields

$$\Delta p_{2I} = \frac{\partial p_2(I_b)}{\partial I_b} \Delta I_b = \alpha p_2(10.33\mu\text{A}) \Delta I_b. \quad (2.6)$$

The uncertainty of  $p_2$  given by bias current fluctuations  $\Delta I_b = 5.0 \text{ nA}$  is  $u_I = \Delta p_{2I} = 6 \times 10^{-4}$ . The value of  $\Delta I_b$  is the average of the standard deviations of all the measured bias currents in the experiment.

### 2.5.6 Temperature fluctuations

The detection probabilities in our experiment are a function of temperature because the working principle of SSPDs is based on a superconducting material whose properties (e.g., critical current  $I_c$  and coherence length  $\xi$ ) are functions of temperature. We use a PID feedback control loop (Lake Shore model 350) to actively stabilize the temperature to  $T_o = 3.2$  K. The measured fluctuations of the temperature in the cryostat are in the range of  $\pm 4$  mK, which we take as the standard deviation of the temperature.

To calculate the influence of the temperature on  $p_2$  at  $10.33 \mu\text{A}$ , we link  $T$  and  $p_2$  via the bias current  $I_b$ . To estimate the fluctuations we use

$$\Delta p_{2T}(T) = \frac{\partial p_2(I_b)}{\partial I_b} \frac{\partial I_b}{\partial T} \Delta T, \quad (2.7)$$

in which the term  $\frac{\partial p_2(I_b)}{\partial I_b}$  has been given by Eq. (2.5), and  $\frac{\partial I_b}{\partial T}$  can be obtained from the observation that the detector is an energy detector [30]. Following Ref. [30], for a certain observed  $p_2$ , the bias current  $I_b$  of the SSPD has a linear relation with the total excitation photon energy  $E$ :

$$I_b(T) = I_o(T) - \gamma E. \quad (2.8)$$

The slope  $\gamma$  is found to be temperature independent and is determined by the properties and geometry of the NbN film [30]. By putting a horizontal line  $p_i = 0.10$  onto Fig. 2.4(a) we get two crossover points:  $I_{b1} = 14.00 \mu\text{A}$  for one 1200 nm photon with  $E_1 = 1.033$  eV, and  $I_{b2} = 10.33 \mu\text{A}$  for two photons with  $E_2 = 2.066$  eV. Using these two points  $(E_1, I_{b1})$  and  $(E_2, I_{b2})$  we estimate  $\gamma = 3.58 \mu\text{A}/\text{eV}$  and  $I_o = 17.72 \mu\text{A}$  at 3.2 K. The temperature-dependent current  $I_o(T)$  has an expression based on Ref. [30, 60]:

$$I_o(T) = I_o(T_o) \frac{\sqrt{1 - T/T_c}}{\sqrt{1 - T_o/T_c}}, \quad (2.9)$$

where  $T_o = 3.2$  K and  $T_c = 9.42$  K. Using above, we calculate the bias of  $p_i$  due to temperature fluctuations around  $T_o = 3.2$  K and  $10.33 \mu\text{A}$ :

$$\Delta p_{2T} = -\frac{1}{2} p_2(10.33 \mu\text{A}) * I_o(3.2\text{K}) \alpha \frac{1}{T_c - T_o} \Delta T. \quad (2.10)$$

The uncertainty of  $p_2$  given by temperature is  $u_T = |\Delta p_{2T}| = 6 \times 10^{-4}$ .

### 2.5.7 Combined standard uncertainty

We have calculated the influence of all uncertainty sources on  $p_2$  for bias current  $10.33 \mu\text{A}$ , and we can compare these calculations to the observed fluctuations in the raw data. We use Eq. (2.3) to create synthetic data that includes all the technical fluctuations, and the contribution due to shot noise.

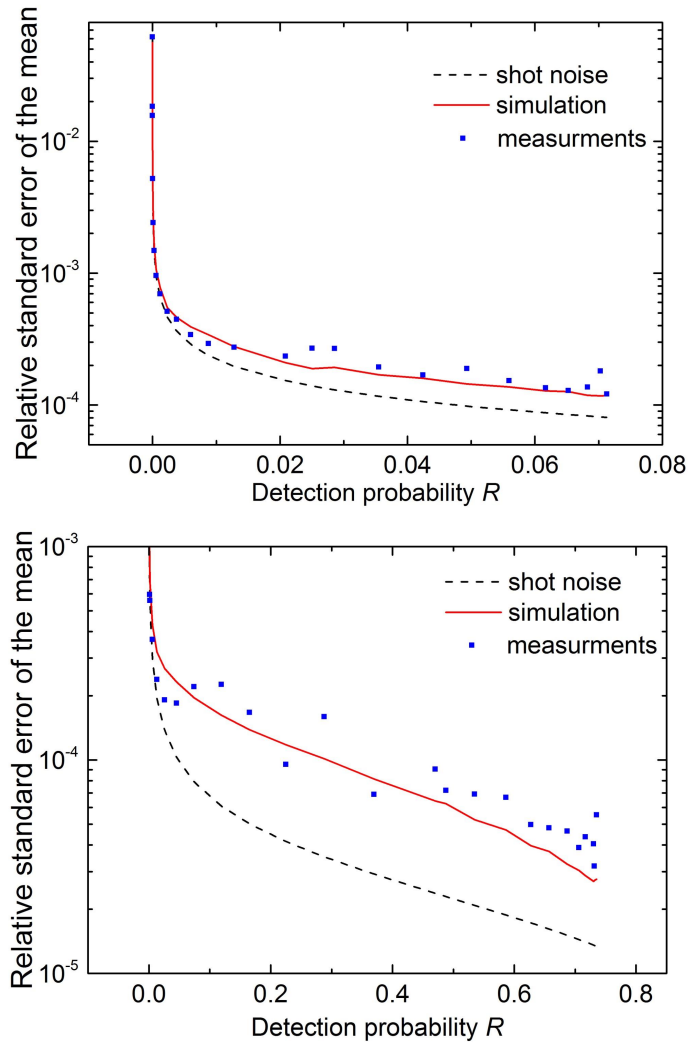


Figure 2.6: The relative standard error of the mean of detection probability ( $SEM/R$ ) at the bias current  $10.33 \mu\text{A}$  (a) and  $14.00 \mu\text{A}$  (b). The symbols represent experimental values. The black dashed curve is the predicted shot noise limit. The red curve takes into account additional fluctuations (laser power, current and temperature fluctuations) present in the experiment.

To incorporate fluctuations in laser power, we multiply the mean photon  $N$  by a factor of  $(1 + \sigma_L \times r)$ . Both temperature and bias current fluctuations affect the probabilities  $\Pi_2$ . To simulate these effects, we add  $r \times \sqrt{\Delta p_{2I}^2 + \Delta p_{2T}^2}$  to  $\Pi_2$ , in which  $p_{2I}$  and  $p_{2T}$  quantify the change in  $\Pi_2$ . The value of  $\Pi_1=0$  remains constant in this example.

Next, we (we already used Eq. (2.3) to create the synthetic data  $R_s$ ) add shot noise given by the binomial distribution as  $r \times \sqrt{R_s(1 - R_s)/tf}$  to  $R_s$ , with  $tf = 2 \times 10^6$ . We repeat the process 1000 times to obtain a set of synthetic data  $R_s$ , from which we calculate the averaged estimated  $\overline{R_s}$  ( $\overline{R_s} = \frac{1}{L} \sum_{j=1}^L R_{s,j}$ ) and the standard error of the mean  $SEM$ .

For bias current  $14.00 \mu\text{A}$  we repeat the same procedure. Figure 2.6 compares the normalized values of  $SEM/R$  for the measured data (blue points) to the simulation (red line) at the two typical currents of  $10.33 \mu\text{A}$  (a) and  $14.00 \mu\text{A}$  (b). The black dashed curve corresponds to the shot noise level. At each of the two currents, for low detection probabilities ( $R < 10^{-2}$ ) the shot noise dominates the measurement, while for larger detection probabilities ( $R > 10^{-2}$ ) the fluctuations due to technical noise sources (i.e., laser power, bias current and temperature) exceed the shot noise. The agreement of the measurement and simulations show that shot noise becomes more important at lower bias current since the overall count rate is lower, and that our experimental tomography operates in the nontrivial regime where technical noise becomes comparable to shot noise.

Table 1 shows all the noise sources and their influences on the internal detection efficiencies. The relative combined uncertainty of  $p_2$  at  $10.33 \mu\text{A}$  and  $p_1$  at  $14.00 \mu\text{A}$  are 1.3% and 2.0%, respectively, which reflects an high accuracy of the QDT procedure in our work. In our experiment laser power fluctuations contribute the most to the total uncertainty for both currents (or one-photon and two-photon regimes). An improvement of the accuracy of the QDT would result from using a more stable laser. However, if we eliminate laser power fluctuations from the error budget, the final relative combined uncertainty is only decreased to 0.9% ( $10.33 \mu\text{A}$ ) and 1.1% ( $14.00 \mu\text{A}$ ), because the other noise sources have a comparable effect on the outcome of QDT. The accuracy can only be significantly improved by minimizing the influences of all other technical noise, e.g., by also optimizing the design of electronic circuit and temperature feedback controlling of cryostat.

## 2.6 Conclusions

We have performed tomography at 1200 nm wavelength on an SSPD using quantum detector tomography and obtained the internal detection efficiency in different photon number regimes. We deliberately added optical loss to the

setup to rigorously demonstrate the separation of overall macroscopic absorption efficiency from the intrinsic, microscopic detection probabilities  $p_i$ .

We find that additional technical noise exists in the measurement, which makes the fluctuations of the noise level higher than shot noise level at detection probabilities  $R > 10^{-2}$ . By limiting the data to this threshold of  $10^{-2}$ , we improve the fit in tomography leading to a decreased value of  $\chi^2$ . The accuracy of the tomography is limited by long time drift in laser power, while short time fluctuations in bias current and temperature have a comparable effect.

We measured fluctuations including laser power, power meter accuracy, bias current, and temperature. The sensitivity of tomography to each of these factors is evaluated either via numerical simulation or via error propagation to quantify the total uncertainty of the  $p_i$ . We find that both  $p_1$  and  $p_2$  can be determined with a small relative uncertainty of 1.3% and 2.0%.

